doi:10.15625/2525-2518/18533



Synthesis of hydroxyapatite and strontium-substituted hydroxyapatite for bone replacement and osteoporosis treatment

Le Thi Bang^{1,*}, Nguyen Van Ha¹, Bui Duc Long¹, Nguyen Thi Hong Nhung²

¹School of Materials Science and Engineering, Hanoi University of Science and Technology, No. 1 Dai Co Viet, Hai Ba Trung, Ha Noi, Viet Nam

²Faculty of Mechanical Engineering, Sao Do University, Chi Linh, Hai Duong, Viet Nam

*Email: bang.lethi@hust.edu.vn

Received: 15 July 2023; Accepted for publication: 15 April 2024

Abstract. Hydroxyapatite (HAp) is an inorganic component exhibiting bioactivity similar to that of natural bone. However, it is not resorbed by osteoclasts during bone remodeling due to its lack of bio-resorption property. This can be enhanced by the substitution of other elements present in bone mineral. In this work, hydroxyapatite (HAp) and strontium-substituted hydroxyapatite (Sr-HAp) were synthesized by a precipitation method. Calcium nitrate tetra hydrate [Ca(NO₃)₂•4H₂O], disodium hydrogen phosphate (Na₂HPO₄), and strontium nitrate [Sr(NO₃)₂] were used as Ca, PO₄ and Sr sources, respectively. The molar ratio Ca/P = 1.67 was used to synthesize HAp, while (Ca+Sr)/P = 1.67 was used to synthesize strontium substituted-HAp (Sr-HAp). The reaction was carried out at room temperature. The results showed that pure HAp and Sr-HAp were formed with nanometer-sized particles. Sr substitution in the HAp lattice resulted in an increase in both the lattice disorder and crystal aspect ratio. The results of *in vitro* bioactive testing using simulated bodily fluids also showed that both HAp and Sr-HAp had high bioactivity, with the Sr-HAp sample having the greater bioactivity. Therefore, the HAp and Sr-HAp have great potential for biological applications.

Keywords: Biomedical application, hydroxyapatite, strontium, osteoporosis treatment.

Classification numbers: 2.7.1

1. INTRODUCTION

Hydroxyaptite $[Ca_{10}(PO_4)_6(OH)_2, HAp]$ has been widely studied and applied in orthopedic and dental applications due to its chemical similarity to the inorganic composition of human bone. The synthesized HAp exhibits various physical and biological characteristics, which depend on factors such as shape, microstructure, and crystallinity. However, the biodegradability of HAp is limited, as it remains in the body for years. This situation can lead to issues like infections or alterations in the mechanical properties of the implanted bone [1, 2].

Furthermore, the HAp is not resorbed by osteoclasts to participate in bone remodeling process, unlike bone minerals [3, 4]. Consequently, the utility of HAp in biomedical applications

is limited. The bioresorption of HAp can be improved by substituting trace elements, i.e. Si, CO₃, Mg, Na, Sr, etc. that are present in the human bone composition [5-7]. These ions substitutions reduce the crystallite size of the HAp and facilitate new bone formation [7-9].

Additionally, bone defects due to osteoporosis in the elderly as the aging population is increasing are common issues in orthopedic surgery. Research has demonstrated that strontium (Sr) in bone promotes bone regeneration, significantly reduces bone resorption, and can treat osteoporosis [8, 10, 11]. Therefore, the development of biomaterials with chemical compositions resembling those of human bones and containing elements that promote bone regeneration is essential for bone replacement.

In this study, the HAp and strontium-substituted hydroxyapatite (Sr-HAp) were synthesized by a precipitation method using calcium nitrate tetrahydrate [Ca(NO₃)₂•4H₂O], disodium hydrogen phosphate (Na₂HPO₄), and strontium nitrate [Sr(NO₃)₂] as precursors. The reaction was carried out at room temperature. The resulting products were characterized using x-ray diffraction (XRD), scanning electron microscopy (SEM), energy dispersive X-ray spectroscopy (EDX), and Fourier transform infrared attenuated total reflection spectroscopy (ATR-FTIR). Furthermore, the bioactivities of the synthesized HAp and Sr-HAp were assessed using the simulated body fluid method.

2. MATERIALS AND METHODS

2.1. Materials

Calcium nitrate tetrahydrate [Ca(NO₃)₂•4H₂O, Xilong, China], disodium hydrogen phosphate [Na₂HPO₄, Xilong, China], strontium nitrate [Sr(NO₃)₂, Xilong, China], and sodium hydroxide [NaOH, Xilong, China] were used to synthesize HAp and Sr-HAp. The chemicals are used directly without purification.

2.2. Methods

In order to synthesize HAp, a solution containing Ca^{2^+} was prepared by dissolving $Ca(NO_3)_2 \cdot 4H_2O$ in distilled water at a concentration of 0.5 mol/L (referred to as calcium solution). Similarly, a solution containing $PO_4^{3^-}$ was also prepared by dissolving $Na_2HPO_4 \cdot 12H_2O$ in distilled water at a concentration of 0.3 mol/L (referred to as phosphate solution). The Ca/P molar ratio was 1.67, corresponding to stoichiometric HAp [12]. The phosphate solution was slowly added dropwise to the calcium solution, and the reaction was homogenized through continuous stirring using a magnetic stirrer (HS4000-S-E, Benchmark, Korea) at 300 rpm for 2 hours. The solution's pH was controlled at pH = 9-10 by adding 2 mol/L NaOH solution to the reaction mixture.

Similarly, for the synthesis of Sr-HAP, an appropriate amount of calcium and phosphate solutions was also prepared to achieve the molar ration of (Ca+Sr)/P = 1.67. The amount of Sr ion was fixed at 5 mmol, assuming that Sr would replace Ca ions in the HAp lattice. Once the reaction was complete, the precipitates were retained in the mother solution and aged at room temperature for 12 hours. The HAp and Sr-HAp precipitates were washed and filtered multiple times with distilled water. The resulting powder was dried at 70 °C for 12 hours and then ground to obtain a fine powder.

The synthesized powders were characterized using an X-ray diffractometer (XRD, AERIS, Netherland) for phase identifications. The molecular structure was investigated using a total

attenuation Fourier transform infrared spectrometer (Thermo Scientific - NICOLET iS50FT-IR). The microstructure of the synthesized powder was observed using a scanning electron microscope (SEM, JEOL JSM-IT200) equipped with an energy dispersive X-ray spectrometer (EDS) under an accelerating voltage of 10 kV.

The crystallite size (d) was calculated using the diffraction peak at approximately 25.8° (20) because it was sharper and isolated from others following the Scherrer equation (1) [13]:

$$d = \frac{K\lambda}{\beta\cos\theta} \tag{1}$$

where: $d = \text{crystallite size } (\dot{A})$; K = a shape factor equal to 0.9; $\lambda = \text{wavelength of Cu } K\alpha$ radiation equal to 1.5406 \dot{A} ; $\theta = \text{half of the diffraction angle, degree}$; $\beta = \text{full width at half maximum } (FWHM)$, rad.

The lattice parameters (a and c) of the hexagonal structure for HAp and Sr-HAp were also calculated using the (hkl) plane of apatite from XRD patterns using the equations for hexagonal structure as follows (2) [13]:

$$\frac{1}{d^2} = \frac{4}{3} \left(\frac{h^2 + hk + k^2}{a^2} \right) + \frac{l^2}{c^2}$$
 (2)

d is the distance between the crystal planes obtained from XRD results at the (002) and (300) Miller plane family of the HAp and Sr-HAp.

The density of the samples was determined using a specific gravity (S.G.). The procedure is as follows: First, an empty 50 mL borosilicate bottle (S.G. bottle) was weighed to measure the dry weight of the bottle (M1). Subsequently, approximately 1 g of HAp and Sr-HAp powders was placed into the S.G. bottle, and the combined weight of S.G. bottle and HAp/Sr-HAp was recorded (M2). Thirdly, deionized water was added to the S.G. bottle until the powders was fully immersed in the water. The entire S.G. bottle was then placed in a vacuum desiccator for 30 min to eliminate any trapped air in the powder. The water level was adjusted to fill the S.G. bottle before sealing it with the lid. The S.G. bottle was wiped and weighed (M3). Subsequently, both the water and powder were removed from the S.G. bottle. Finally, the S.G. bottle was filled with deionized water, covered with the lid, and weighed again (M4).

The density of HAp/Sr-HAp powder was then calculated from the formula below:

$$\rho_{\text{powder}} = \frac{M_2 - M_1}{(M_4 - M_1) - (M_3 - M_2)} \times \rho_{\text{H}_2\text{O}}$$

where ρ_{H_2O} is taken as 1.0 g/cm³ at room temperature.

The bioactivity of the HAp and Sr-HAp samples was assessed by immersing them in simulated body fluid (SBF) for 7 days, following Kokubo's principle [14]. For this experiment, apatite pellets (10 mm diameter) were prepared by compacting 300 mg of HAp and Sr-HAp powders at room temperature through uniaxial pressing at 20 MPa, followed by heat treatment at 500 °C (Lenton 1500, England) for 2 hours. This low temperature was selected to dense pellets without phase decomposition. The SBF solution was refreshed every 2 days. After immersion, the sample was taken out from the SBF and carefully rinsed with deionized water. Subsequently, the sample was dried in a desiccator for 48 hours without applying heat. The formation of apatite on the surface of the sample was confirmed by scanning electron microscopy (SEM).

3. RESULTS AND DISCUSSION

Figure 1 shows the XRD patterns of various samples. The XRD patterns of the synthesized HAp and Sr-HAp perfectly matched those of the HAp standard. Moreover, the diffraction peaks of the Sr-HAp sample were less intense than those of the HAp sample. This may due to the substitution of Sr into the HAp lattice, resulting in an increase in the crystallite size of HAp. The crystallite sizes of the samples were calculated using Scherrer equation [13]. The crystallite size of the HAp sample was 15.08 nm, while that of Sr-HAp was approximately 9.59 nm.

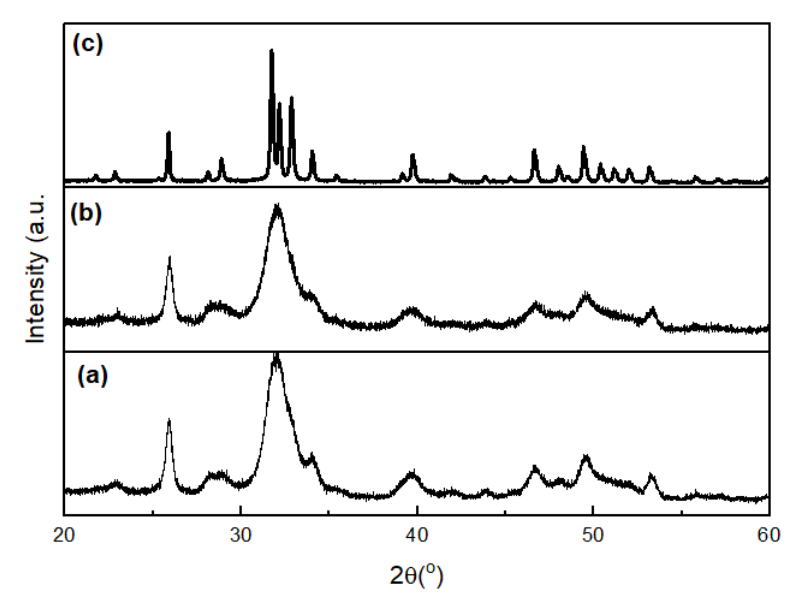


Figure 1. XRD patterns of different samples: (a) Hydroxyapatite (HAp), (b) Sr-substituted Hydroxyapatite (HAp), (c) Hydroxyapatite (HAp) standard (PDF No. 9-432).

The parameters of a- and c-axes for the synthesized HAp were 9.639 Å and 6.898 Å, respectively, while those of Sr-HAp were 9.662 Å (a-axis) and 6.903 Å (c-axis). The substitution of Sr in the HAp structure led to an increase in the lattice parameters. This increase was attributed to the larger atomic radius of Sr ion (0.113 nm) compared to that of Ca ion (0.099 nm) [15]. These results are consistent with previous studies showing that both a- and c-axes increased with Sr substitution [16, 17].

The XRD analysis was suported by the IR spectra. As shown in Figure 2, the IR spectra of HAp and Sr-HAp exhibited characteristic features of the HAp phase, when compared with the spectrum of the HAp standard. Regardless of Sr substitution, the IR spectra of both samples displayed the typical bands of phosphate groups at approximately 561 cm⁻¹ (v_4), 602 cm⁻¹ (v_4), 9602 cm⁻¹ (v_1), and and 1027 - 1089 cm⁻¹ (v_3) [16, 18, 19]. The hydroxide groups in the structure were detected at about 630 cm⁻¹ (v_1). It should be noted that, the substitution of Sr in HAp leads to a reduction in the intensity of the OH groups, resulting in a broader OH absorbance at approximately 630 cm⁻¹ compared to that of pure HAp. A similar result was observed in a previous study [20]. Therefore, it can be concluded that Sr was substituted into the HAp lattice structure.

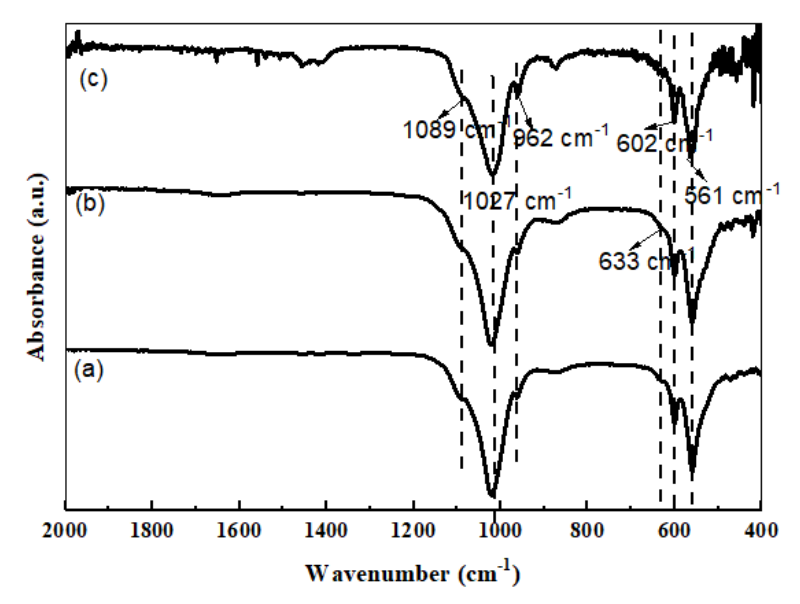


Figure 2. IR patterns of different samples: (a) Hydroxyapatite (HAp), (b) Sr-substituted Hydroxyapatite (HAp), (c) Hydroxyapatite (HAp) standard.

Figure 3 shows the SEM images of the synthesized HAp and Sr-HAp samples at various magnifications.

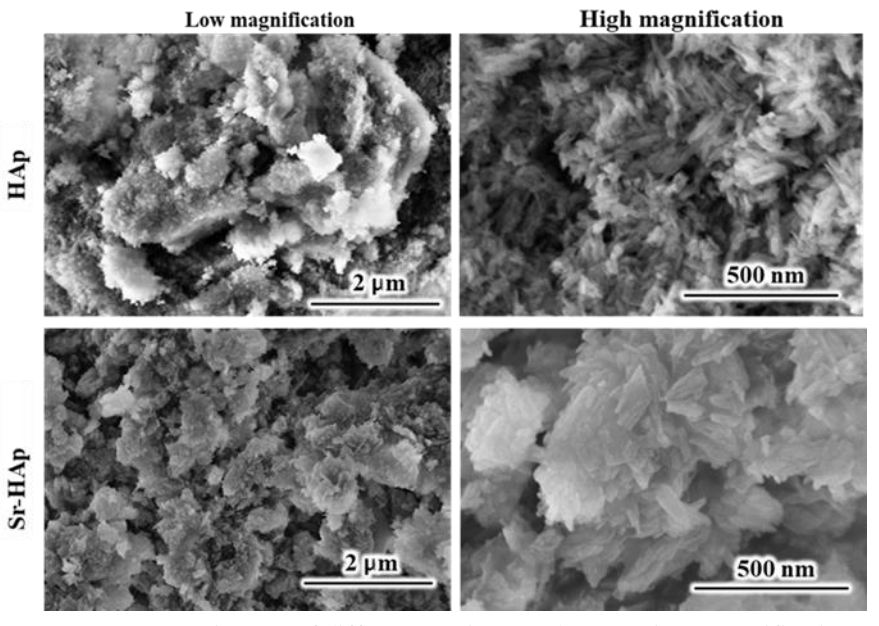


Figure 3. SEM images of different apatite samples at various magnifications.

SEM scans at low magnification revealed that the synthesized powders consisted of agglomerates or lumps. These agglomerated powders formed due to the agglomeration of fine particles with high surface energy that tended to clump together. Both HAp and Sr-HAp crystals exhibited a needle-like or rod-like shapes, as observed in high magnification SEM images. The primary particles observed were nanosized crystals. The nanocrystals of HAp were measured to

be approximately 20 nm in width and about 100 nm in length, while those of Sr-HAp were about 22 nm in width and 126 nm in length. The aspect ratios (length/width) of HAp and Sr-HAp were 4.8 and 5.7, respectively. It has been reported that higher aspect ratios could lead to improved biological properties of synthesized hydroxyapatite [21].

Figure 4 shows the EDS spectra and the quantities of Ca, P, and Sr elements in different samples. These results indicate that the powder was composed of Ca, P, and Sr ions in the structure. It is worth noting that NaOH forms in the reactions and might contribute to sodium contamination in the powder.

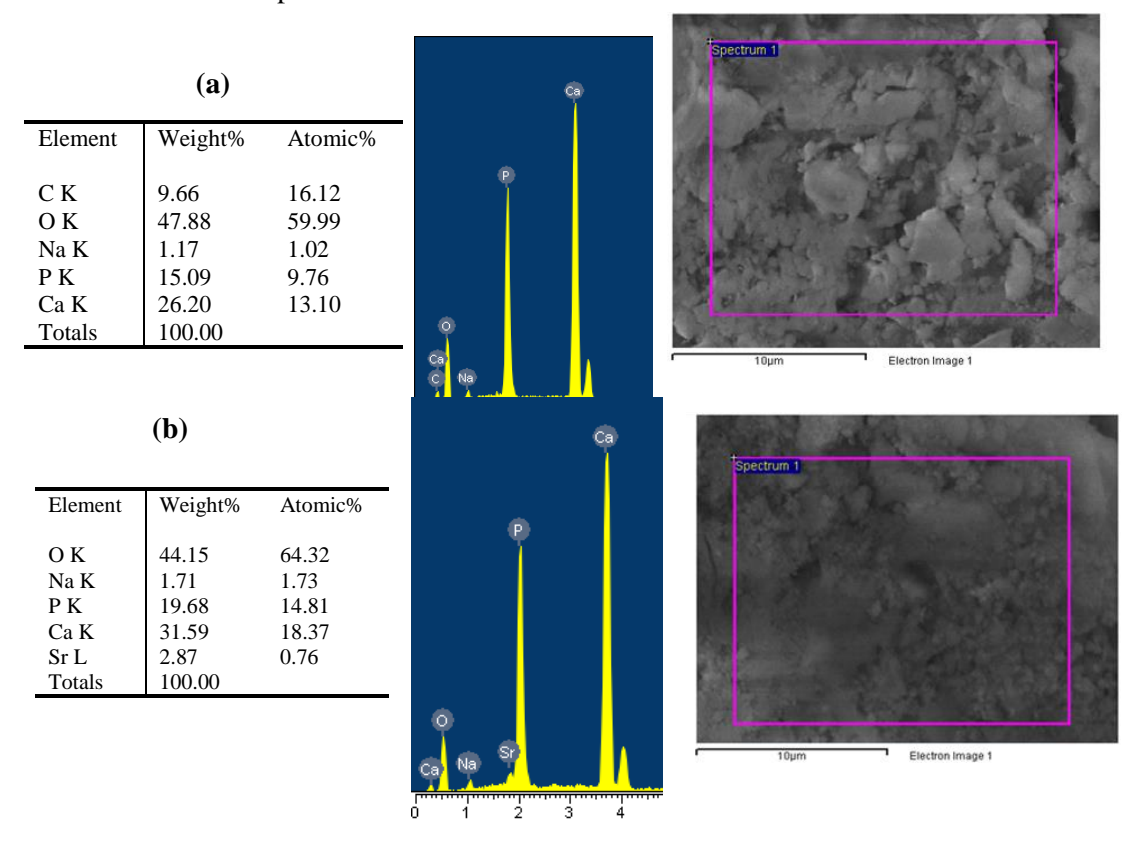


Figure 4. EDX results of different apatite samples: (a) HAp, (b) Sr-HAp.

As detected by the EDS, the amount of Sr substitution in the apatite structure was approximately 2.87 wt%. The substitution of strontium ions for calcium ions in HAp would reduce the calcium concentration in the apatite structure leading to a reduction in the Ca/P ratio [22, 23]. Therefore, the change in Ca/P ratios was attributed to the substitution of Sr in the HAp crystals.

It should be noted that the Sr amount, as well as Ca/P ratios as detected by the EDS are solely for screening purposes to indicate the presence of Sr in the apatite structure. Therefore, for a more accurate investigation, an appropriate characterization method, such as ICP-MS, could be considered.

The densities of HAp and Sr-HAp powders were also determined using the S.G. method. The substitution of Sr led to a reduction in the density of the HAp powder, with the densities of HAp and Sr-HAp being 1.9 g/cm³ and 1.6 g/cm³, respectively.

The bioactivity of HAp and Sr-HAp were evaluated through the simulated body fluid (SBF) method [24]. Figure 5 shows the surface morphology after immersion for 7 days. It's evident that cauliflower-like apatite layer was observed in both samples. Interestingly, the Sr-HAp sample exhibited a thicker apatite layer during the same immersion period. It is widely acknowledged that a majority of bioactive materials develop an apatite layer on their surfaces when suspended in SBF for a specific period. Consequently, the formation of an apatite layer on these samples confirms their bioactive nature, indicating that the synthetic surface establishes a chemical bond with the host bone after implantation,

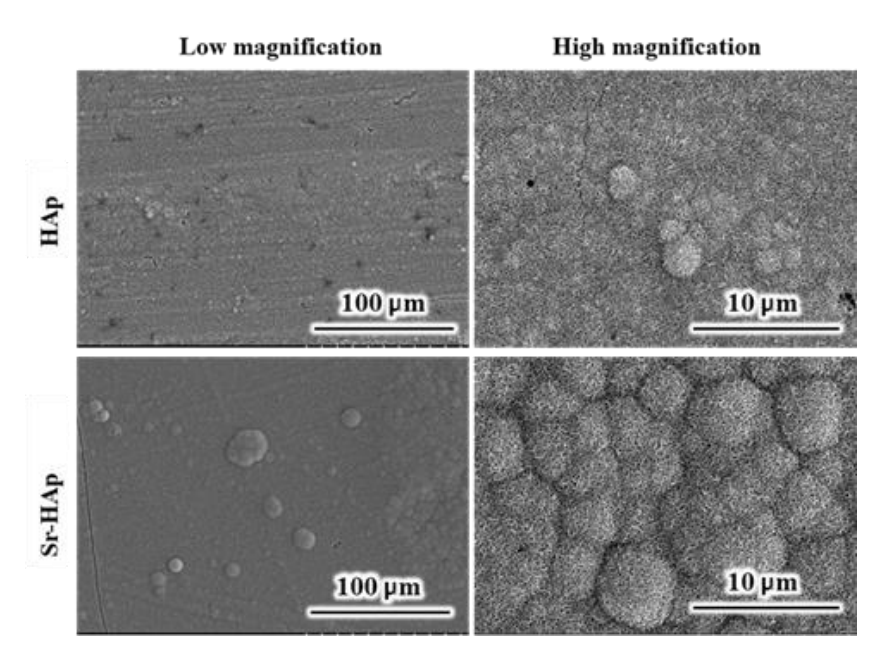


Figure 5. SEM images of HAp and Sr-HAp surfaces after immersion in SBF for 7 days.

The mechanism of apatite layer formation is the result of dissolution and precipitation processes. Upon immersion, the surface partially dissolves, releasing Ca²⁺, HPO₄²⁻, PO₄³⁻, and Sr²⁺ to the solution. As the concentration of these ions reaches the supersaturation level with respect to apatite, they precipitate, forming apatite nanocrystals on the surface of the material [24]. The thickening of the apatite layer could arise from accelerated dissolution and precipitation. The substitution of Sr into the HAp lattice is known to enhance the solubility of HAp [25]. The heightened solubility leads to a more rapid dissolution rate. As a result, Sr substitution enhanced the bioactive process, thereby potentially improving osteointegration *in vivo*.

4. CONCLUSIONS

Hydroxyapatite (HAp) and strontium-substituted hydroxyapatite (Sr-HAp) powders were successfully synthesized using a precipitation method at room temperature. It was observed that the substitution of Sr in HAp influenced the structural order and increased the aspect ratios of the HAp crystals. The powders were in the nanosize range, approximately 20 nm in width, with notable agglomeration. Furthermore, the Sr addition led to a decrease in the Ca/P molar ratio and a reduction in the density of the HAp. The *in vitro* bioactivity assessment using the SBF

method demonstrated that the Sr-HAp exhibited superior bioactive property compared to pure HAp.

Acknowledgements. This research work is funded by the Vietnam National Foundation for Science and Technology Development (NAFOSTED) under grant number 104.03-2020.36.

CRediT authorship contribution statement. Le Thi Bang: Methodology, Investigation, Funding acquisition, First draft manuscript. Nguyen Van Ha: Methodology, Data analysis. Bui Duc Long: Formal analysis, Supervision. Nguyen Thi Hong Nhung: Data analysis.

Declaration of competing interest. The authors declare that they have no known competing financial interests or personal relationships that could have appeared to influence the work reported in this paper.

REFERENCES

- 1. Ishikawa K. Bone Substitute Fabrication Based on Dissolution-Precipitation Reactions. Materials **3** (2) (2010), 1138-1155. 10.3390/ma3021138.
- 2. Ishikawa K. -Carbonate Apatite Bone Replacement, in Handbook of Bioceramics and Biocomposites, I.V. Antoniac, Editor 2016, Springer International Publishing: Cham. p. 213-232.
- 3. Ishikawa K. and Hayashi K. Carbonate apatite artificial bone, Science and Technology of Advanced Materials **22** (1) (2021), 683-694. 10.1080/14686996.2021.1947120.
- 4. Madupalli H., Pavan B., and Tecklenburg M. M. J. Carbonate substitution in the mineral component of bone: Discriminating the structural changes, simultaneously imposed by carbonate in A and B sites of apatite, Journal of Solid State Chemistry **255** (2017) 27-35. https://doi.org/10.1016/j.jssc.2017.07.025.
- 5. Arkin V. H., Narendrakumar U., Madhyastha H., and Manjubala I. Characterization and In Vitro Evaluations of Injectable Calcium Phosphate Cement Doped with Magnesium and Strontium, ACS Omega 6 (4) (2021), 2477-2486. 10.1021/acsomega.0c03927.
- Bang L. T., Ramesh S., Purbolaksono J., Ching Y. C., Long B. D., Chandran H., and Othman R. - Effects of silicate and carbonate substitution on the properties of hydroxyapatite prepared by aqueous co-precipitation method, Materials & Design 87 (2015) 788-796. https://doi.org/10.1016/j.matdes.2015.08.069.
- 7. Kim Y., Kwon S., and Roh Y. Effect of Divalent Cations (Cu, Zn, Pb, Cd, and Sr) on Microbially Induced Calcium Carbonate Precipitation and Mineralogical Properties, Frontiers in Microbiology **12** (2021). 10.3389/fmicb.2021.646748.
- 8. Kołodziejska B., Stępień N., and Kolmas J. The Influence of Strontium on Bone Tissue Metabolism and Its Application in Osteoporosis Treatment, Int. J. Mol. Sci. **22** (12) (2021) 6564. 10.3390/ijms22126564.
- 9. Karunakaran G., Cho E.B., Kumar G. S., Kolesnikov E., Janarthanan G., Pillai M. M., Rajendran S., Boobalan S., Sudha K. G., and Rajeshkumar M. P. Mesoporous Mg-doped hydroxyapatite nanorods prepared from bio-waste blue mussel shells for implant applications, Ceramics International **46** (18, Part A) (2020) 28514-28527. https://doi.org/10.1016/j.ceramint.2020.08.009.
- 10. Wu Q., Hu L., Yan R., Shi J., Gu H., Deng Y., Jiang R., Wen J., and Jiang X. Strontium-incorporated bioceramic scaffolds for enhanced osteoporosis bone regeneration, Bone Research 10 (1) (2022) 55. https://doi.org/10.1038/s41413-022-00224-x.

- 11. Stipniece L., Wilson S., Curran J. M., Chen R., Salma-Ancane K., Sharma P. K., Meenan B. J., and Boyd A. R. Strontium substituted hydroxyapatite promotes direct primary human osteoblast maturation, Ceramics International **47** (3) (2021) 3368-3379. https://doi.org/10.1016/j.ceramint.2020.09.182.
- 12. Ishikawa K., Matsuya S., Miyamoto Y., and Kawate K. 9.05 Bioceramics, in Comprehensive Structural Integrity, I. Milne, R.O. Ritchie, and B. Karihaloo, Editors. 2003, Pergamon: Oxford. p. 169-214.
- 13. Cullity B. D. -Elements of X-Ray Diffraction, 2nd ed., 1978, Addison-Wesley: Philipines.
- 14. Kokubo T. and Takadama H. Simulated Body Fluid (SBF) as a Standard Tool to Test the Bioactivity of Implants, in Handbook of Biomineralization, 2007, p. 97-109.
- 15. Capuccini C., Torricelli P., Boanini E., Gazzano M., Giardino R., and Bigi A. Interaction of Sr-doped hydroxyapatite nanocrystals with osteoclast and osteoblast-like cells, J. Biomed Mater Res. A **89** (3) (2009) 594-600.
- 16. Bigi A., Boanini E., Capuccini C., and Gazzano M. Strontium-substituted hydroxyapatite nanocrystals, Inorganica Chimica Acta **360** (3) (2007) 1009-1016. https://doi.org/10.1016/j.ica.2006.07.074.
- 17. Kavitha M., Subramanian R., Narayanan R., and Udhayabanu V. Solution combustion synthesis and characterization of strontium substituted hydroxyapatite nanocrystals, Powder Technology **253** (2014), 129-137. https://doi.org/10.1016/j.powtec.2013.10.045.
- 18. Sakai A., Valanezahad A., Ozaki M., Ishikawa K., and Matsuya S. Preparation of Srcontaining carbonate apatite as a bone substitute and its properties, Dent Mater J. **31** (2) (2012) 197-205.
- 19. Hajji H., Le Gallet S., Saviot L., Ben Salem E., and Millot N. Mechanosynthesis of carbonate and lithium co-substituted hydroxyfluorapatite. Materials Research Bulletin, **150** (2022) 111750. https://doi.org/10.1016/j.materresbull.2022.111750.
- 20. Terra J., Dourado E. R., Eon J.-G., Ellis D. E., Gonzalez G., and Rossi A. M. The structure of strontium-doped hydroxyapatite: an experimental and theoretical study, Physical Chemistry Chemical Physics **11** (3) (2009), 568-577. 10.1039/b802841a.
- 21. Chen S., Pujari-Palmer S., Rubino S., Westlund V., Ott M., Engqvist H., and Xia W. Highly repeatable synthesis of nHA with high aspect ratio, Materials Letters **159** (2015) 163-167. https://doi.org/10.1016/j.matlet.2015.06.086.
- 22. Abert J., Bergmann C., and Fischer H. Wet chemical synthesis of strontium-substituted hydroxyapatite and its influence on the mechanical and biological properties, Ceramics International **40** (7, Part A) (2014) 9195-9203. https://doi.org/10.1016/j.ceramint. 2014.01.138.
- 23. Suganthi R. V., Elayaraja K., Joshy M. I. A., Chandra V. S., Girija E. K., and Kalkura S. N. Fibrous growth of strontium substituted hydroxyapatite and its drug release, Materials Science and Engineering: C **31** (3) (2011) 593-599. https://doi.org/10.1016/j.msec.2010.11.025.
- 24. Kokubo T. and Takadama H. -Simulated Body Fluid (SBF) as a Standard Tool to Test the Bioactivity of Implants, 2008. p. 97-109.
- 25. Ressler A., Žužić A., Ivanišević I., Kamboj N., and Ivanković H. Ionic substituted hydroxyapatite for bone regeneration applications: A review, Open Ceramics **6** (2021) 100122. https://doi.org/10.1016/j.oceram.2021.100122.